The Kelvin-Voigt Model's Suitability to Explain the Viscoelastic Properties of Anticorrosion Bitumen at Large Shear Strain in Subsea Cables and Umbilicals

Magnus Komperød[1]

[1]Technological Analyses Centre, Nexans Norway AS, Norway, magnus.komperod@nexans.com

Abstract

Bitumen is used as anticorrosion to protect steel armor wires in subsea cables and umbilicals. Bitumen's viscoelastic behavior influences the mechanical properties of the cables, in particular the bending stiffness. UFLEX2D is a software tool for mechanical analyses of cables and similar structures, which can include the viscoelastic effect of bitumen using a Kelvin-Voigt model. This paper evaluates how well the Kelvin-Voigt model is able to resemble bitumen's viscoelastic properties. It is concluded that the Kelvin-Voigt model's lack of temperature dependence can be managed, while the model's handling of strain amplitude is too simple to fully explain bitumen's behavior. It is also concluded that the Kelvin-Voigt model has limited abilities to resemble the frequency response of bitumen.

Keywords: Arctic Engineering; Bitumen; Bode Diagram; Cross Section Analysis; Kelvin-Voigt Model; Offshore Technology; Rheology; Subsea Cable; Umbilical.

1 Introduction

Umbilicals are cable-like structures consisting of electric and fiber optic signal cables, as well as steel tubes for transportation of fluids and for running subsea hydraulic equipment. Power umbilicals also include electric power phases for energizing subsea electric units, such as compressors. Umbilicals are essential for offshore oil and gas production.

Connecting power grids across seas requires subsea power cables. Such cables consist of one or several power phases, where each phase is a stranded conductor made of copper or aluminum covered by an electric insulation system. Subsea power cables are also used in direct electrical heating (DEH) systems, which is a technology for flow assurance in oil and gas pipelines. Please refer to Nysveen et al. (2007) for an introduction to DEH systems. Figure 1 shows a DEH riser cable having four phases, each consisting of a stranded copper conductor with a XLPE insulation system.

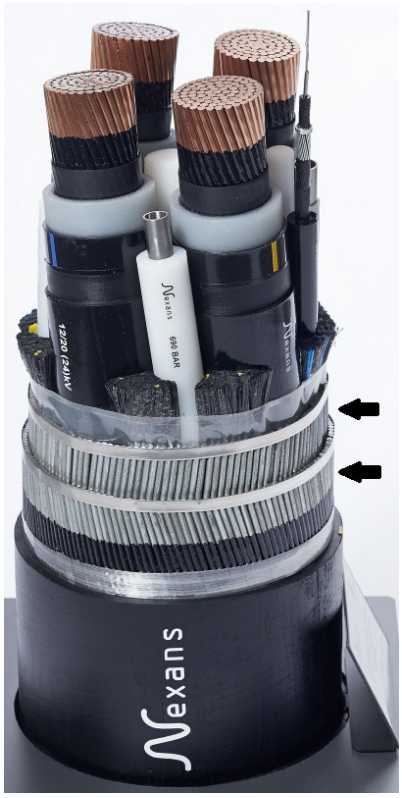

Figure 1. DEH riser cable with four phases. The cable also includes steel tubes and fiber optic signal cables. The two black arrows in the figure indicate the two layers of galvanized steel armor wires.

Umbilicals and subsea cables commonly include armor wires, which main purpose is to carry the cable's axial load and thereby reduce the axial tension in the other cable elements. Armor wires may also be used to tune the cable's submerged-weight-to-diameter ratio, which influences the cable's dynamic behavior in the sea. Armor wires are usually arranged in one to four armor layers, which are located right inside the cable's outer sheath. The two black arrows in Figure 1 indicate the two layers of armor wires in the DEH riser cable.

Armor wires are commonly made of galvanized steel. This material has favorable mechanical properties and is

cost-effective. However, as the steel wires are constantly submerged in seawater, the galvanization may be insufficient corrosion protection. Therefore the armor wires may be coated in bitumen, which serves as corrosion protection.

Because bitumen is a viscoelastic material it changes the shear forces between the armor wires and their neighboring cable elements, compared to the frictional shear forces that arise when bitumen is not present on the contact surfaces. Shear forces between cable elements due to friction and how these shear forces influence the cables' mechanical properties are extensively covered in the literature. See for example Féret and Bournazel (1987) and Kebadze (2000).

Literature on how shear forces of bitumen and other viscoelastic materials influence cables is sparse. Olsen et al. (2014), Konradsen and Ouren (2014), and Komperød et al. (2015) cover identification of bitumen's viscoelastic properties. The latter paper focuses on identification of bitumen's properties at equally large shear strain as in real-life cables. Mullins et al. (2015) develop models of the force required to pull an bitumen-coated armor wire out of a cable. Hedlund (2015) models the bending moment vs. bending curvature characteristics for cables with bitumen-coated armor wires. The latter work is based on Mullins et al. (2015). Also, some work on this issue has been carried out by MARINTEK as part of the implementation of bitumen's viscoelastic properties in the UFLEX2D software. Please refer to Appendix A for a brief note on UFLEX2D.

For mechanical cable models to include the effect of bitumen, these models must include material models of bitumen's viscoelastic properties. The UFLEX2D software uses the Kelvin-Voigt model to describe these properties. The contribution of the present paper is to evaluate how well the Kelvin-Voigt model is able to explain the viscoelastic properties of bitumen identified in Komperød et al. (2015).

2 Nomenclature

Table 1 presents the nomenclature used in this paper. Complex numbers are indicated with tilde, for example $\tilde{G}$. The following notation applies to the shear strain: γ is the shear strain as function of t. γ_0 is the center-to-peak amplitude of γ. $\tilde{\gamma}$ is the phase vector (phasor) notation of γ. Similar notation is used for the shear stress, τ.

When it is essential to distinguish between G^* and φ of the Kelvin-Voigt model vs. G^* and φ of the empirical model, the subscripts KV and E are used. When at no risk of confusion, the angular frequency, ω, may be referred to as the frequency.

Table 1. Nomenclature.

c_i, d_i	Parameters of the empirical model.
$\tilde{G}$	Bitumen's complex shear modulus [Pa].
G^*	Bitumen's shear stress amplitude to shear strain amplitude ratio [Pa].
G^*_{E}	G^* as modeled by the empirical model [Pa].
G^*_{KV}	G^* as modeled by the Kelvin-Voigt model [Pa].
G'	Bitumen's storage modulus [Pa].
G''	Bitumen's loss modulus [Pa].
j	Imaginary unit [-], $j^2 \stackrel{\text{def}}{=} -1$.
T	Temperature of bitumen [°C].
T_1	Specific value of T used in examples [°C].
t	Time [s].
γ, γ_0, $\tilde{\gamma}$	Bitumen's shear strain [-].
γ_1	Specific value of γ_0 used in examples [-].
η	Bitumen's viscosity [Pa s].
τ, τ_0, $\tilde{\tau}$	Bitumen's shear stress [Pa].
φ	Phase shift between shear stress and shear strain of bitumen [rad].
φ_{E}	φ as modeled by the empirical model [rad].
φ_{KV}	φ as modeled by the Kelvin-Voigt model [rad].
ω	Angular frequency [rad/s].
ω_1, ω_2	Specific values of ω used in examples [rad/s].

3 Properties of the Kelvin-Voigt Model

The Kelvin-Voigt model is on the form

$$\tau(t) = G'\gamma(t) + \eta\frac{\mathrm{d}\gamma(t)}{\mathrm{d}t}, \tag{1}$$

where G' is the material's shear storage modulus and η is its viscosity. The Kelvin-Voigt model is a linear, time-invariant (LTI) model as the model parameters G' and η are time-invariant, and

DOI 10.3384/ecp15119319

$$G'\left(a\gamma_1(t)+b\gamma_2(t)\right)+\eta\frac{\mathrm{d}}{\mathrm{d}t}\left(a\gamma_1(t)+b\gamma_2(t)\right) \tag{2}$$
$$=a\left(G'\gamma_1(t)+\eta\frac{\mathrm{d}\gamma_1(t)}{\mathrm{d}t}\right)+b\left(G'\gamma_2(t)+\eta\frac{\mathrm{d}\gamma_2(t)}{\mathrm{d}t}\right).$$

Eq. 2 states that the response of the input sequence $a\gamma_1(t)+b\gamma_2(t)$ is equal to a times the response of the input sequence γ_1 plus b times the response of the input sequence γ_2. Hence, the Kelvin-Voigt model obeys the superposition principle.

3.1 Behavior at Sinusoidal Strain

Assume that the strain is applied in a sinusoidal manner. The strain can then be written as

$$\gamma(t)=\gamma_0\cos(\omega t), \tag{3}$$

where γ_0 is the center-to-peak amplitude and ω is the angular frequency. Inserting Eq. 3 into Eq. 1 gives

$$\begin{aligned}\tau(t)&=G'\gamma_0\cos(\omega t)+\eta\frac{\mathrm{d}}{\mathrm{d}t}\gamma_0\cos(\omega t) \qquad (4)\\ &=G'\gamma_0\cos(\omega t)-\eta\omega\gamma_0\sin(\omega t)\\ &=G'\gamma_0\cos(\omega t)-G''\gamma_0\sin(\omega t).\end{aligned}$$

In the third line of Eq. 4 the shear loss modulus is introduced as $G''\stackrel{\text{def}}{=}\eta\omega$.

Euler's formula is

$$e^{jx}=\cos(x)+j\sin(x), \tag{5}$$

which gives

$$\begin{aligned}e^{-jx}&=\cos(-x)+j\sin(-x) \qquad (6)\\ &=\cos(x)-j\sin(x).\end{aligned}$$

Solving Eqs. 5 and 6 for $\cos(x)$ and $\sin(x)$ gives the well-known identities

$$\cos(x)=\frac{e^{jx}+e^{-jx}}{2}, \tag{7}$$

$$\sin(x)=\frac{e^{jx}-e^{-jx}}{2j}. \tag{8}$$

Inserting Eqs. 7 and 8 into Eq. 4

$$\begin{aligned}\tau(t)&=G'\gamma_0\frac{e^{j\omega t}+e^{-j\omega t}}{2}-\eta\omega\gamma_0\frac{e^{j\omega t}-e^{-j\omega t}}{2j} \qquad (9)\\ &=G'\gamma_0\frac{e^{j\omega t}+e^{-j\omega t}}{2}+j\eta\omega\gamma_0\frac{e^{j\omega t}-e^{-j\omega t}}{2}\\ &=\frac{\gamma_0}{2}\left[(G'+j\eta\omega)e^{j\omega t}+(G'-j\eta\omega)e^{-j\omega t}\right]\\ &=\frac{\gamma_0}{2}G^*_{\mathrm{KV}}\left[e^{j\varphi_{\mathrm{KV}}}e^{j\omega t}+e^{-j\varphi_{\mathrm{KV}}}e^{-j\omega t}\right]\\ &=\gamma_0 G^*_{\mathrm{KV}}\frac{e^{j(\omega t+\varphi_{\mathrm{KV}})}+e^{-j(\omega t+\varphi_{\mathrm{KV}})}}{2}\\ &=\gamma_0 G^*_{\mathrm{KV}}\cos(\omega t+\varphi_{\mathrm{KV}}).\end{aligned}$$

On the forth line of Eq. 9, the factors $(G'\pm j\eta\omega)$ are written on polar form where the follow notation is used

$$\begin{aligned}G^*_{\mathrm{KV}}&\stackrel{\text{def}}{=}\sqrt{G'^2+\eta^2\omega^2} \qquad (10)\\ &=G'\sqrt{1+\left(\frac{\eta}{G'}\right)^2\omega^2},\end{aligned}$$

$$\varphi_{\mathrm{KV}}\stackrel{\text{def}}{=}\arctan\left(\frac{\eta}{G'}\omega\right). \tag{11}$$

The physical interpretations are that G^* is the shear stress amplitude to shear strain amplitude ratio, and φ is the phase shift between the shear stress and the shear strain. These interpretations are valid for any model, while the calculations of G^*_{KV} and φ_{KV} from Eqs. 10 and 11 are specific to the Kelvin-Voigt model.

The derivatives of G^*_{KV} and φ_{KV} w.r.t. ω will be used later in this paper. These derivatives are

$$\frac{\mathrm{d}G^*_{\mathrm{KV}}}{\mathrm{d}\omega}=\frac{\eta^2\omega}{\sqrt{G'^2+\eta^2\omega^2}}, \tag{12}$$

$$\frac{\mathrm{d}\varphi_{\mathrm{KV}}}{\mathrm{d}\omega}=\frac{\eta}{G'\left(1+\left(\frac{\eta}{G'}\right)^2\omega^2\right)}. \tag{13}$$

The sinusoidal functions $\gamma(t)$ of Eq. 3 and $\tau(t)$ of Eq. 9 can be written on phase vector (phasor) form as

$$\tilde{\gamma}=\gamma_0 e^{j\omega t}, \tag{14}$$

$$\tilde{\tau}=\gamma_0 G^* e^{j(\omega t+\varphi)}. \tag{15}$$

The complex shear modulus, $\tilde{G}$, is defined as the ratio of these phase vectors, i.e.

$$\begin{aligned}\tilde{G} &\stackrel{\text{def}}{=} \frac{\tilde{\tau}}{\tilde{\gamma}} \\ &= \frac{\gamma_0 G^* e^{j(\omega t+\varphi)}}{\gamma_0 e^{j\omega t}} \\ &= G^* e^{j\varphi} \\ &= G' + j\eta\omega.\end{aligned} \tag{16}$$

The upper three rows of Eq. 16 apply to any model, while the forth row is specific to the Kelvin-Voigt model.

Figure 2 shows a Bode diagram of the Kelvin-Voigt model based on Eqs. 10 and 11. From physics, it is known that both parameters G' and η are non-negative. The second line of Eq. 10, as well as Eq. 11, tell how the Bode diagram will be influenced by changing the parameters: Increasing (decreasing) the ratio $\frac{\eta}{G'}$ will shift the Bode diagram to the left (to the right). Increasing (decreasing) both parameters with the same factor, so that G' increases (decreases), while the ratio $\frac{\eta}{G'}$ is fixed, will shift the magnitude plot upward (downward). In other words: *The Bode diagram may be shifted by changing the parameters, but its shape will always be as illustrated in Figure 2*. The only exceptions are (i) $\eta = 0$, which gives $G^*_{\text{KV}} = G'$ and $\varphi = 0$ for any ω, and (ii) $G' = 0$, which gives $G^*_{\text{KV}} = \eta\omega$ and $\varphi = \frac{\pi}{2}$ rad, i.e. 90°, for any ω.

The asymptotic behavior is also inherent in the Kelvin-Voigt model and can not be changed by changing the parameters (except for the special cases $G' = 0$ and $\eta = 0$):

1. At low frequencies G^*_{KV} will approach G'.
2. At low frequencies the phase shift, φ_{KV}, will approach 0 rad.
3. At high frequencies G^*_{KV} will approach $\eta\omega$.
4. At high frequencies φ_{KV} will approach $\frac{\pi}{2}$ rad, i.e. 90°.
5. As seen from Eq. 12, G^*_{KV} has a stationary point at $\omega = 0$, and is strictly increasing with ω for $\omega > 0$, provided that $\eta > 0$.
6. As seen from Eq. 13, φ_{KV} is strictly increasing with ω, provided that $\eta > 0$.

This means that any material which viscoelastic properties violate the Bode diagram of Figure 2 and / or the asymptotic behaviors described above can not be correctly modeled by the Kelvin-Voigt model.

4 Bitumen's Properties at Large Shear Strain

This section explains bitumen's viscoelastic properties at large shear strain based on the results of Komperød et al. (2015).

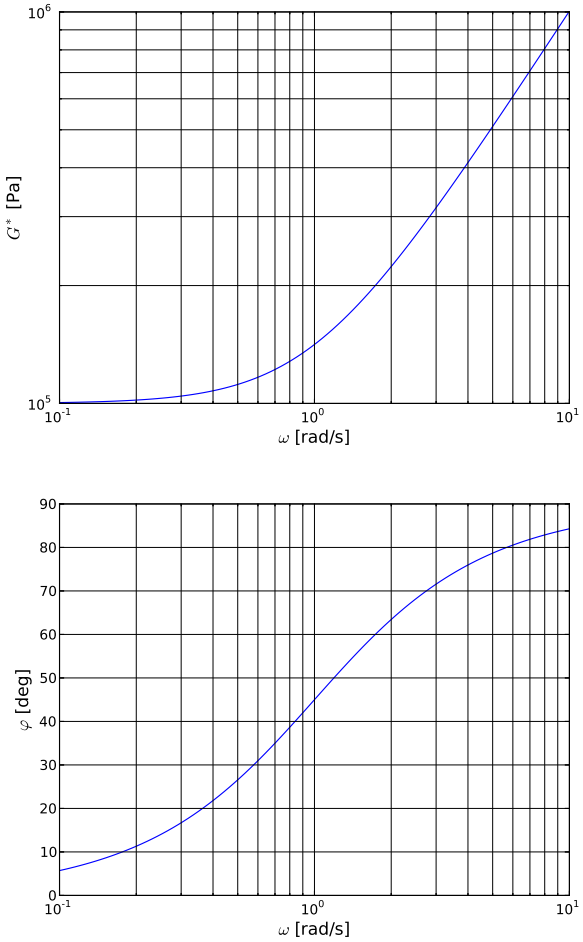

Figure 2. Bode diagram of the Kelvin-Voigt model using the parameters $G' = 1.0 \times 10^5$ and $\eta = 1.0 \times 10^5$. Please note that the second axis (y-axis) of the phase plot is scaled in [deg], while [rad] is used in the calculations of the main text.

4.1 Model Identification

The author and his colleagues have developed a new laboratory instrument for identification of bitumen's viscoelastic properties, G^* and φ. The advantage of the new laboratory instrument compared to traditional low-strain rheometers is that the new laboratory instrument can measure the viscoelastic properties of bitumen subject to equally large shear strain as in real-life cables. The shear strain of traditional low-strain rheometers is much smaller than the shear strain in cables. Hence, the viscoelastic properties identified in such rheometers may not be representative for bitumen's behavior in cables.

Komperød et al. (2015) present the basic principle of the new laboratory instrument and derive how to calculate bitumen's viscoelastic properties from the sensor measurements of the laboratory instrument. Komperød et al. (2015) also present an empirical model of G^*_{E} and φ_{E} as function of the shear strain amplitude, γ_0, the angular frequency, ω, and the bitumen temperature, T. This model is based on experiments in the new laboratory instrument

DOI 10.3384/ecp15119319

which was run for 48 different combinations of γ_0, ω, and T. Two parallels were run for each of the 48 combinations, i.e. in total 96 experiments were run.

The model identified from these 96 experiments is

$$G^*_{\mathrm{E}} = c_0 - c_1\gamma_0 + c_2\gamma_0\omega - c_3 T + c_4 T^2, \quad (17)$$

$$\varphi_{\mathrm{E}} = d_0 + d_1\gamma_0 - d_2\omega + d_3 T. \quad (18)$$

In Eqs. 17 and 18, c_i and d_i are real, positive parameters, which are identified using the ordinary least squares method (OLS). That is, for each of the 96 experiments, γ_0, ω, and T are known inputs to the laboratory instrument, while one value for G^*_{E} and one value for φ_{E} are identified from each experiment. Hence, the experiment output G^*_{E} and the regressors γ_0, $\gamma_0\omega$, T, and T^2 are known for 96 experiments, which are used to identify the parameters c_0, c_1, c_2, c_3, and c_4 using OLS. Similarly, the experiment output φ_{E} and the regressors γ_0, ω, and T are also known for 96 experiments, which are used to identify the parameters d_0, d_1, d_2, and d_3 using OLS.

The model of Eqs. 17 and 18 is a simple, empirical model, which model structure is chosen to ensure numerical convergence and to be simple to give practical interpretations. It is emphasized that the model structure is not based on analytical models of bitumen's properties. However, the model gives reasonable explanation of bitumen's behavior within the operating range of the laboratory experiments. Please refer to Komperød et al. (2015) for detailed explanation of the model identification and model validation.

4.2 Model Interpretation

In Eq. 17, c_0 is a constant term. The term $-c_1\gamma_0$ expresses that G^* will decrease as the shear strain amplitude increases. That is, the shear stress amplitude will grow slower than the shear strain amplitude.

The product $\gamma_0\omega$ expresses bitumen's strain rate (strain per time unit). Hence, the term $c_2\gamma_0\omega$ means that bitumen will set up larger shear forces if it is strained rapidly than if strained slowly.

The first and second derivatives of G^*_{E} w.r.t T are

$$\frac{\partial G^*_{\mathrm{E}}}{\partial T} = -c_3 + 2c_4 T, \quad (19)$$

$$\frac{\partial^2 G^*_{\mathrm{E}}}{\partial T^2} = 2c_4. \quad (20)$$

The first derivative is negative for the temperature range covered by the laboratory experiments. This means that bitumen will set up larger shear forces at lower temperatures than at higher temperatures for the same strain. Hence, bitumen will behave more like a "glue" as the temperature decreases. As seen from Eq. 20, the second derivative is positive for all values of T. This means that the first derivative will become more negative as the temperature decreases. In other words, G^*_{E} grows with increasing rate as the temperature decreases.

As emphasized in Komperød et al. (2015), G^*_{E} does not depend directly on the frequency, ω, but on the product $\gamma_0\omega$, which expresses the strain rate.

Eq. 18 is straight forward to interpret: The phase shift, φ_{E}, increases for increased strain amplitude, γ_0, and for increased temperature, T. For increased frequency, ω, the phase shift will decrease.

4.3 Comparison with the Kelvin-Voigt Model

Comparing the empirical model, i.e. Eqs. 17 and 18, which is based on laboratory experiments, with the Kelvin-Voigt model of Eqs. 10 and 11 shows some significant differences:

1. In the empirical model both G^*_{E} and φ_{E} depend on the temperature, while the Kelvin-Voigt model does not include temperature-dependence at all. Hence, a set of Kelvin-Voigt model parameters, G' and η, can only be valid for one single temperature, not a temperature interval.

   If the Kelvin-Voigt model is to be used for variable temperatures, the model parameters G' and η must be adjusted to the temperature variations. This may be implemented as the parameters being continuous functions of the temperature, i.e. $G' = G'(T)$ and $\eta = \eta(T)$. Tables may also be used, where G' and η are listed for various temperature points. Interpolation may be used between these temperature points.

2. In the empirical model G^*_{E} and φ_{E} also depend on the strain amplitude, γ_0, while the Kelvin-Voigt model does not depend on γ_0. This is a bigger issue than the temperature-dependence discussed above, because it is reasonable (with a few exceptions) to assume that the temperature is nearly homogeneous over a pitch length of the cable. However, bitumen's shear strain varies significantly over a pitch length: It is largest at the cable's neutral axis of bending and zero at the points farthest away from the neutral axis.

3. As discussed above, Eq. 17 shows that G^*_{E} of the empirical model depends on the strain rate, which is expressed through the product $\gamma_0\omega$, but G^*_{E} does not depend on the frequency, ω, alone. Comparing with G^*_{KV} of the Kelvin-Voigt model, Eq. 10, shows that this model depends only on ω, not on the product $\gamma_0\omega$.

   This issue means that if the strain amplitude, γ_0, is constant, G^*_{E} of the empirical model and G^*_{KV} of the Kelvin-Voigt model will depend on the frequency, ω. But if γ_0 is allowed to vary, the behaviors of the two models will differ. As explained above, the strain amplitude will be largest at the cable's neutral axis of

bending and zero farthest away from the neutral axis. Hence, the assumption of constant strain amplitude over a pitch length of the cable will not be met in a real-life cable.

4. For the empirical model, the derivative of G^*_{E} w.r.t. ω is

$$\frac{\partial G^*_{\mathrm{E}}}{\partial \omega} = c_2 \gamma_0. \tag{21}$$

Comparing Eq. 21 with Eq. 12 shows that the two derivatives are quite different. $\frac{\partial G^*_{\mathrm{KV}}}{\partial \omega}$ depends on the frequency, ω, while $\frac{\partial G^*_{\mathrm{E}}}{\partial \omega}$ depends on the strain amplitude, γ_0. However, both derivatives are positive, which means that G^* is strictly increasing with the frequency for both models (expect that the Kelvin-Voigt model has a stationary point at $\omega = 0$). Also, for both models, $\frac{\partial G^*}{\partial \omega}$ is constant w.r.t. ω for high frequencies. That is, G^* increases proportional with ω for high ω.

5. Inspecting Eq. 18 shows that the terms d_0, $d_1\gamma_0$, and $d_3 T$ give positive contributions to the phase shift, φ_{E}. The contribution from the term $-d_2\omega$ is zero for $\omega = 0$ and strictly decreasing for increasing ω. Hence, the phase shift has a positive value given by $d_0 + d_1\gamma_0 + d_3 T$ for $\omega = 0$, and thereafter decreases as ω increases. However, for the frequency range covered by the empirical model, the phase shift is always positive.

   The behavior of the Kelvin-Voigt model is very different from the empirical model w.r.t. the phase shift. The phase shift of the Kelvin-Voigt model is given by Eq. 11. The function $\arctan(\cdot)$ is zero when the argument is zero and then increases towards its asymptote of $\frac{\pi}{2}$ in a strictly increasing, nonlinear manner as the argument increases.

   The phase shift of the empirical model is positive for zero frequency and then decreases for increasing frequency, while the phase shift of the Kelvin-Voigt model is zero for zero frequency and then increases for increasing frequency. Therefore, although the two models are very different w.r.t. phase shift, the phase shift graphs of the models will cross each other at one specific frequency. Hence, the Kelvin-Voigt model can resemble the phase shift of the empirical model at one single point in the frequency domain. However, the Kelvin-Voigt model can never resemble the empirical model over any frequency interval, because the models' derivative w.r.t. frequency always have opposite signs (plus or minus).

For the empirical model of Eq. 17, the derivative of G^*_{E} w.r.t. the strain amplitude, γ_0, is

$$\frac{\partial G^*_{\mathrm{E}}}{\partial \gamma_0} = -c_1 + c_2\omega. \tag{22}$$

Setting Eq. 22 equal to 0 and solving for ω gives $\omega = \frac{c_1}{c_2}$. Hence, for this particular frequency, G^*_{E} becomes insensitive to the strain amplitude, γ_0. That is, for this frequency the issue of higher strain amplitude at the cable's neutral axis of bending than farther away from the neutral axis will vanish, because G^*_{E} is insensitive to γ_0 if $\omega = \frac{c_1}{c_2}$. This desirable frequency is somewhat higher than the frequency of the cable's cyclic behavior as hanging from an offshore installation. Still, the effect that the term $c_2\omega$ counteracts the term $-c_1$ is favorable.

Figure 3 shows a Bode diagram of a Kelvin-Voigt model, as well as an empirical model on the form of Eqs. 17 and 18. The Kelvin-Voigt model has the same model parameters as in Figure 2. The magnitude plot shows that the G^* graphs of the two models behave somewhat similarly, but are not identical. The φ graphs of the two models are very different, which is in accordance to point 5 above. However, as predicted, the phase shift graphs cross each other, meaning they yield the same phase shift at one specific frequency, in this case at $\omega = 1$.

5 Fitting the Kelvin-Voigt Model to the Empirical Model

The issues discussed in Section 4.3 conclude that the Kelvin-Voigt model can not resemble the empirical model over a frequency interval. In particular the phase shift, φ, fits poorly as the Kelvin-Voigt model and the empirical model have opposite signs of $\frac{\partial \varphi}{\partial \omega}$. Still, as will be shown below, the Kelvin-Voigt model is suitable if only one specific frequency is to be modeled, not a frequency interval. Further, if the phase shift is disregarded, then G^*_{KV} of the Kelvin-Voigt model can resemble G^*_{E} of the empirical model well over a limited frequency range.

Mathematically speaking, the two Kelvin-Voigt model parameters, G' and η, provide two degrees of freedom for how to fit the Kelvin-Voigt model to the empirical model. In other words: Two requirements, formulated as two equations, can be met.

5.1 Fitting G^*_{KV} and φ_{KV} for one Specific ω

Assume that the model parameters c_i and d_i of Eqs. 17 and 18 are identified from laboratory experiments or otherwise. The problem addressed in this section is how to calculate the parameters of the Kelvin-Voigt model, G' and η, so that the Kelvin-Voigt model resembles the empirical model for a specific strain amplitude, γ_1, a specific frequency, ω_1, and a specific temperature, T_1. This means that the two requirements to be met can be expressed as

DOI 10.3384/ecp15119319

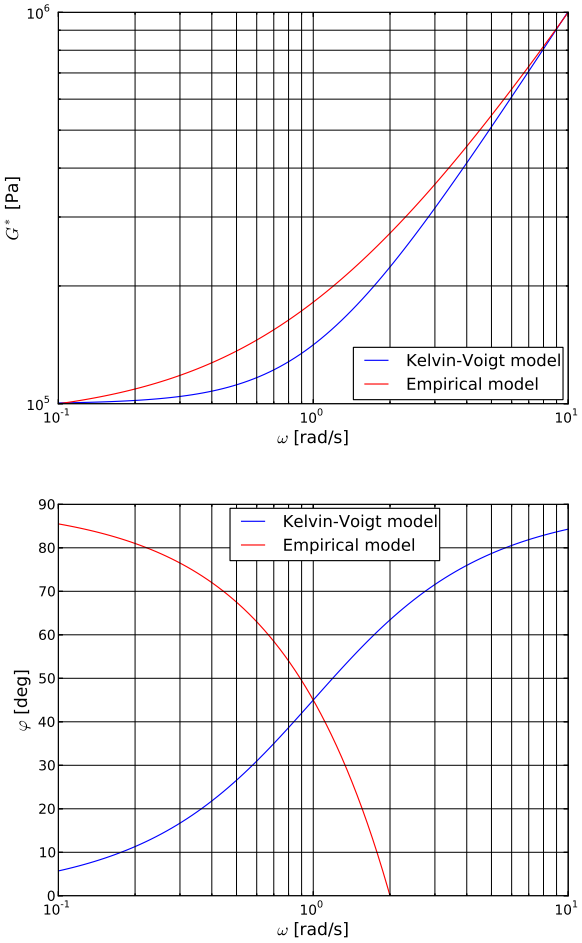

Figure 3. Bode diagram of a Kelvin-Voigt model and an empirical model. The Kelvin-Voigt model has the same model parameters as in Figure 2.

$$G^*_{\mathrm{KV}}(\omega_1) = G^*_{\mathrm{E}}(\gamma_1, \omega_1, T_1), \tag{23}$$

$$\varphi_{\mathrm{KV}}(\omega_1) = \varphi_{\mathrm{E}}(\gamma_1, \omega_1, T_1), \tag{24}$$

where the right hand side of these equations are obtained by inserting γ_1, ω_1, and T_1 into Eqs. 17 and 18.

The next issue is to solve for the Kelvin-Voigt parameters G' and η. Inserting Eq. 24 and $\omega = \omega_1$ into Eq. 11 and rewriting gives

$$\tan(\varphi_{\mathrm{E}}) = \frac{\eta}{G'}\omega_1. \tag{25}$$

Inserting Eqs. 23 and 25 into Eq. 10

$$\begin{aligned} G^*_{\mathrm{E}} &= G'\sqrt{1+\tan^2(\varphi_{\mathrm{E}})} \\ &= G'\sqrt{1+\frac{\sin^2(\varphi_{\mathrm{E}})}{\cos^2(\varphi_{\mathrm{E}})}} \\ &= G'\sqrt{\frac{\cos^2(\varphi_{\mathrm{E}})}{\cos^2(\varphi_{\mathrm{E}})}+\frac{\sin^2(\varphi_{\mathrm{E}})}{\cos^2(\varphi_{\mathrm{E}})}} \\ &= G'\sqrt{\frac{\cos^2(\varphi_{\mathrm{E}})+\sin^2(\varphi_{\mathrm{E}})}{\cos^2(\varphi_{\mathrm{E}})}} \\ &= G'\sqrt{\frac{1}{\cos^2(\varphi_{\mathrm{E}})}} \\ &= \frac{G'}{\cos(\varphi_{\mathrm{E}})}, \end{aligned} \tag{26}$$

which gives

$$G' = G^*_{\mathrm{E}}\cos(\varphi_{\mathrm{E}}). \tag{27}$$

Inserting Eq. 27 into Eq. 25

$$\tan(\varphi_{\mathrm{E}}) = \frac{\sin(\varphi_{\mathrm{E}})}{\cos(\varphi_{\mathrm{E}})} = \frac{\eta}{G^*_{\mathrm{E}}\cos(\varphi_{\mathrm{E}})}\omega_1, \tag{28}$$

which gives

$$\eta = \frac{G^*_{\mathrm{E}}\sin(\varphi_{\mathrm{E}})}{\omega_1}. \tag{29}$$

Hence, Eqs. 27 and 29 provide explicit expressions for the Kelvin-Voigt model parameters, G' and η, which are based on G^*_{E} and φ_{E} calculated by the empirical model.

Example 1 The parameters of the Kelvin-Voigt model are to be calculated so that the Kelvin-Voigt model resembles the empirical model at the frequency $\omega_1 = 0.5$ for some specified values of strain amplitude, γ_1, and temperature, T_1.

Solution: $\omega = 0.5$ as well as the specified values of γ_1 and T_1 are inserted in Eqs. 17 and 18. These equations then provide G^*_E and φ_E for $\omega = 0.5$. Then insert the calculated G^*_E and φ_E, as well as $\omega_1 = 0.5$, into Eqs. 27 and 29 to obtain the Kelvin-Voigt model parameters G' and η. Figure 4 shows Bode diagram of the Kelvin-Voigt model with the new parameters. Although the graphs of the Kelvin-Voigt model and the empirical model are very different, both G^* and φ match perfectly for $\omega = 0.5$. End of Example 1.

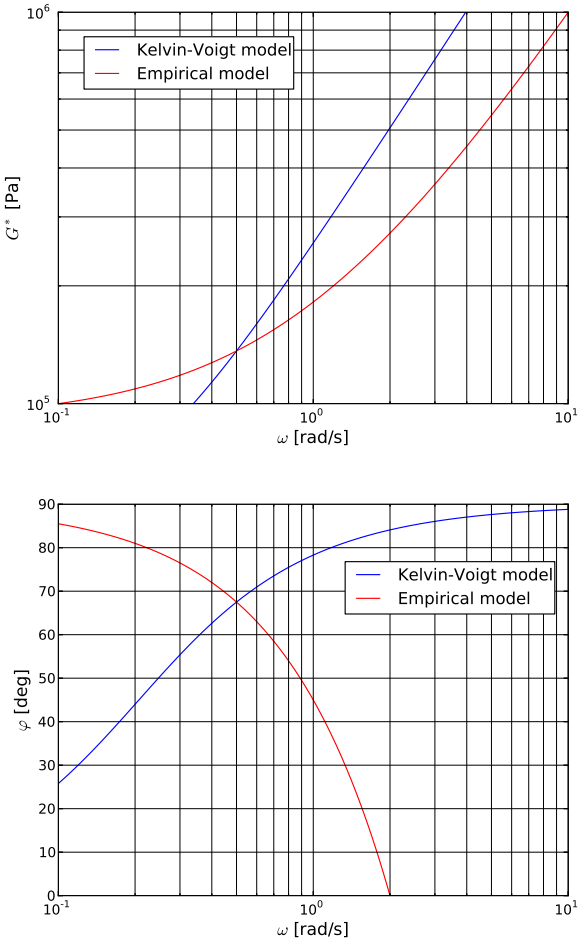

Figure 4. Bode diagram of the Kelvin-Voigt model obtained in Example 1.

5.2 Fitting G^*_{KV} as a First Order Taylor Polynomial

The method proposed in Section 5.1 tunes the parameters G' and η to make the Kelvin-Voigt model resemble both G^*_E and φ_E of the empirical model at one specific frequency, ω_1. However, as seen from Figure 4, the Kelvin-Voigt model fits the empirical model poorly for any frequency that is not very close to ω_1.

The present section suggests an alternative approach to the method of Section 5.1. That is to disregard the fit of φ_{KV} for the benefit of better fit for G^*_{KV}. By better fit, it is here meant that G^*_{KV} of the Kelvin-Voigt model shall resemble the empirical model well not only in one single frequency point, but over a limited frequency interval. As two requirements can be met, these requirements are chosen as:

$$G^*_{KV}(\omega_1) = G^*_E(\gamma_1, \omega_1, T_1), \tag{30}$$

$$\left.\frac{dG^*_{KV}}{d\omega}\right|_{\omega=\omega_1} = \left.\frac{\partial G^*_E}{\partial \omega}\right|_{\gamma_0=\gamma_1, \omega=\omega_1, T=T_1}. \tag{31}$$

Eq. 30 means that G^*_{KV} of the Kelvin-Voigt model and G^*_E of the empirical model shall have the same value at the chosen frequency. This requirement is identical as in Section 5.1. Eq. 31 means that the slope of G^*_{KV} of the Kelvin-Voigt model and the slope of G^*_E of the empirical model shall be identical at the chosen frequency, ω_1.

As seen from Eq. 17, G^*_E is a linear function in ω (the apparent curvature of G^*_E in the Bode diagrams arises because the diagrams have logarithmic axes). Hence, Eqs. 30 and 31 above mean that G^*_E is mathematically equivalent to the linearization, i.e. the first order Taylor expansion, of G^*_{KV}.

As in Section 5.1, the strain amplitude, γ_1, the frequency, ω_1, and the temperature, T_1, which the Kelvin-Voigt model shall be valid for must be chosen and inserted into Eq. 17, which provides the value of G^*_E. The derivative $\frac{\partial G^*_E}{\partial \omega}$ of the empirical model is $c_2\gamma_0$, which becomes $c_2\gamma_1$ after inserting $\gamma_0 = \gamma_1$.

Eqs. 30 and 31 are then inserted into Eqs. 10 and 12, respectively. These equations are then solved for the Kelvin-Voigt parameters, G' and η, as follows: Inserting Eq. 10 into Eq. 12 gives

$$\left.\frac{\partial G^*_E}{\partial \omega}\right|_{\omega=\omega_1} = \frac{\eta^2\omega_1}{G^*_E(\omega_1)}, \tag{32}$$

$$\eta^2 = \frac{G^*_E(\omega_1)}{\omega_1}\left.\frac{\partial G^*_E}{\partial \omega}\right|_{\omega=\omega_1}, \tag{33}$$

$$\eta = \sqrt{\frac{G^*_E(\omega_1)}{\omega_1}\left.\frac{\partial G^*_E}{\partial \omega}\right|_{\omega=\omega_1}}. \tag{34}$$

Squaring Eq. 10 and inserting Eq. 33

DOI 10.3384/ecp15119319

$$G_{\mathrm{E}}^*(\omega_1)^2 = G'^2 + \frac{G_{\mathrm{E}}^*(\omega_1)}{\omega_1}\left.\frac{\partial G_{\mathrm{E}}^*}{\partial \omega}\right|_{\omega=\omega_1} {\omega_1}^2, \tag{35}$$

$$G'^2 = G_{\mathrm{E}}^*(\omega_1)\left(G_{\mathrm{E}}^*(\omega_1) - \left.\frac{\partial G_{\mathrm{E}}^*}{\partial \omega}\right|_{\omega=\omega_1}\omega_1\right), \tag{36}$$

$$G' = \sqrt{G_{\mathrm{E}}^*(\omega_1)\left(G_{\mathrm{E}}^*(\omega_1) - \left.\frac{\partial G_{\mathrm{E}}^*}{\partial \omega}\right|_{\omega=\omega_1}\omega_1\right)}. \tag{37}$$

From Eq. 17 it is trivial to verify that the factor inside the parenthesis of Eq. 37 is equal to G_{E}^* for $\omega = 0$. Further, because $\frac{\partial G_{\mathrm{E}}^*}{\partial \omega} \geq 0$, the expressions inside the square roots of Eqs. 34 and 37 are ensured to be nonnegative if $G_{\mathrm{E}}^* \geq 0$ for $\omega = 0$. Hence, Eqs. 34 and 37 provide the Kelvin-Voigt model parameters that satisfy Eqs. 30 and 31.

Example 2 The parameters of the Kelvin-Voigt model are to be calculated so that the Kelvin-Voigt model resembles G_{E}^* and $\frac{\partial G_{\mathrm{E}}^*}{\partial \omega}$ of the empirical model at the frequency $\omega_1 = 0.5$ for some specified values of strain amplitude, γ_1, and temperature, T_1.

Solution: $\omega = 0.5$ as well as the specified values of γ_1 and T_1 are inserted in Eqs. 17 to obtain G_{E}^*. Further, $\frac{\partial G_{\mathrm{E}}^*}{\partial \omega}$ is calculated as $c_2\gamma_1$. Then the calculated G_{E}^* and $\frac{\partial G_{\mathrm{E}}^*}{\partial \omega}$, as well as $\omega_1 = 0.5$, are inserted into Eqs. 34 and 37, which provide the Kelvin-Voigt model parameters G' and η. The Bode diagram of the Kelvin-Voigt model with the new parameters is shown in Figure 5. The magnitude plot shows that G_{KV}^* of the Kelvin-Voigt model resembles the empirical model well over a limited interval centered at $\omega = 0.5$. As the two models have different second derivatives, $\frac{\partial^2 G^*}{\partial \omega^2}$, the two models will eventually drift apart as moving away from the point $\omega = 0.5$. The cost of this improvement of G_{KV}^* is that the phase shift, φ_{KV}, fits poorly at $\omega = 0.5$ as shown in Figure 5. End of Example 2.

It is seen from Figure 5 that G_{KV}^* is larger than G_{E}^* for all ω, except for $\omega = 0.5$, where $G_{\mathrm{KV}}^* = G_{\mathrm{E}}^*$. The following proves that this inequality always holds. From Taylor's theorem (see for example Section 10.9 of Thomas et al. (2010)) it follows that G_{KV}^* can be written as

$$G_{\mathrm{KV}}^*(\omega) = G_{\mathrm{KV}}^*(\omega_1) + \left.\frac{\mathrm{d}G_{\mathrm{KV}}^*}{\mathrm{d}\omega}\right|_{\omega=\omega_1}(\omega-\omega_1) + \frac{1}{2}\left.\frac{\mathrm{d}^2 G_{\mathrm{KV}}^*}{\mathrm{d}\omega^2}\right|_{\omega=\omega_c}(\omega-\omega_1)^2, \tag{38}$$

where $\omega_1 < \omega_c < \omega$ if $\omega_1 < \omega$, and $\omega < \omega_c < \omega_1$ if $\omega_1 > \omega$.

As G_{E}^* is a linear function in ω, it can be written as

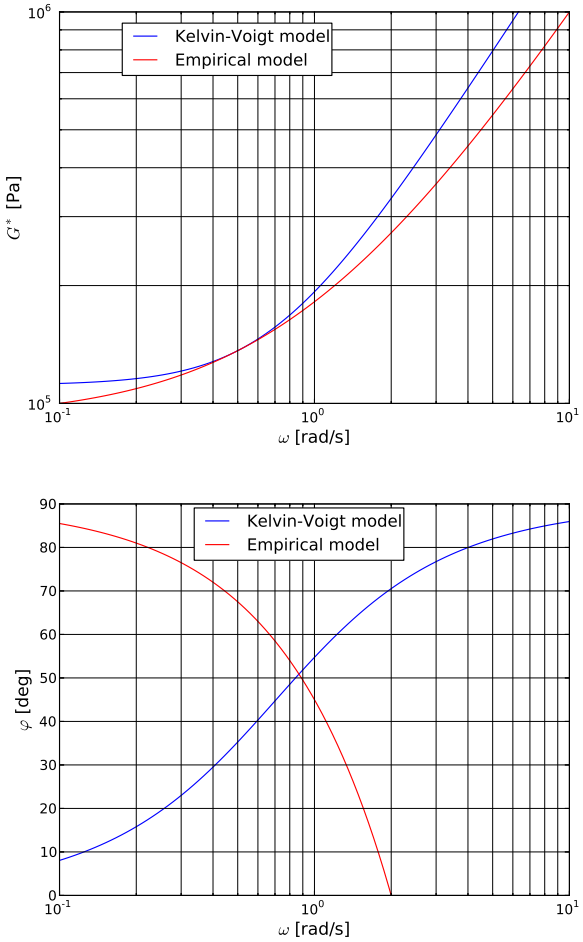

Figure 5. Bode diagram of the Kelvin-Voigt model obtained in Example 2.

$$G_{\mathrm{E}}^*(\omega) = G_{\mathrm{E}}^*(\omega_1) + \frac{\partial G_{\mathrm{E}}^*}{\partial \omega}(\omega-\omega_1). \tag{39}$$

Subtracting Eq. 39 from Eq. 38, and using Eqs. 30 and 31 gives

$$G_{\mathrm{KV}}^*(\omega) - G_{\mathrm{E}}^*(\omega) = \frac{1}{2}\left.\frac{\mathrm{d}^2 G_{\mathrm{KV}}^*}{\mathrm{d}\omega^2}\right|_{\omega=\omega_c}(\omega-\omega_1)^2. \tag{40}$$

The second derivative of G_{KV}^* is

$$\frac{\mathrm{d}^2 G_{\mathrm{KV}}^*}{\mathrm{d}\omega^2} = \frac{G'^2\eta^2}{\left(G'^2+\eta^2\omega^2\right)^{\frac{3}{2}}}, \tag{41}$$

which is positive for any finite ω. Hence, the right hand side of Eq. 40 is positive for any ω and for any ω_c, except for $\omega = \omega_1$, where the right hand side is zero. The practical interpretation of this result is that G_{KV}^* is larger than G_{E}^* for any frequency, ω, except for $\omega = \omega_1$, where $G_{\mathrm{KV}}^* = G_{\mathrm{E}}^*$. In many cases, large G^* will give conservative analysis results. Hence, for these cases the approach presented in this section is conservative.

5.3 Fitting G^*_{KV} at Two Frequencies

In Section 5.2, the two requirements to decide the parameters of the Kelvin-Voigt model are that G^* and $\frac{\partial G^*}{\partial \omega}$ should be equal for the Kelvin-Voigt model as for the empirical model at some specified frequency, ω_1. The present section derives an alternative method to the method of Section 5.2. The two requirements of the method of the present section are that G^*_{KV} of the Kelvin-Voigt model shall resemble the empirical model at two different frequencies, ω_1 and ω_2, where $\omega_2 > \omega_1$. That is

$$G^*_{\mathrm{KV}}(\omega_1) = G^*_{\mathrm{E}}(\gamma_1, \omega_1, T_1), \tag{42}$$

$$G^*_{\mathrm{KV}}(\omega_2) = G^*_{\mathrm{E}}(\gamma_1, \omega_2, T_1). \tag{43}$$

The strain amplitude, γ_1, and the temperature, T_1, which the Kelvin-Voigt model shall be valid for must be chosen and inserted into Eq. 17. Then by also inserting the two frequencies ω_1 and ω_2 in Eq. 17, the equation provides the values for $G^*_{\mathrm{E}}(\omega_1)$ and $G^*_{\mathrm{E}}(\omega_2)$.

Next, Eqs. 42 and 43 are inserted into Eq. 10, together with $\omega = \omega_1$ and $\omega = \omega_2$, respectively. Squaring Eq. 10 then gives

$$G^*_{\mathrm{E}}(\omega_1)^2 = G'^2 + \eta^2 {\omega_1}^2, \tag{44}$$

$$G^*_{\mathrm{E}}(\omega_2)^2 = G'^2 + \eta^2 {\omega_2}^2. \tag{45}$$

Solving Eqs. 44 and 45 for the Kelvin-Voigt parameters G' and η yields

$$G' = \sqrt{\frac{G^*_{\mathrm{E}}(\omega_1)^2 {\omega_2}^2 - G^*_{\mathrm{E}}(\omega_2)^2 {\omega_1}^2}{{\omega_2}^2 - {\omega_1}^2}}, \tag{46}$$

$$\eta = \sqrt{\frac{G^*_{\mathrm{E}}(\omega_2)^2 - G^*_{\mathrm{E}}(\omega_1)^2}{{\omega_2}^2 - {\omega_1}^2}}. \tag{47}$$

It can be mathematically proved that the expressions under the square roots of Eqs. 46 and 47 are nonnegative. These proofs are omitted here. Hence, Eqs. 46 and 47 provide the model parameters of the Kelvin-Voigt model.

Example 3 The parameters of the Kelvin-Voigt model are to be calculated so that G^*_{KV} resembles G^*_{E} at the frequencies $\omega_1 = 0.2$ and $\omega_2 = 1$ for some specified values of strain amplitude, γ_1, and temperature, T_1.

Solution: γ_1 and T_1, as well as ω_1 and ω_2, are inserted into Eq. 17 to obtain $G^*_{\mathrm{E}}(\omega_1)$ and $G^*_{\mathrm{E}}(\omega_2)$. Then the calculated $G^*_{\mathrm{E}}(\omega_1)$ and $G^*_{\mathrm{E}}(\omega_2)$, as well as ω_1 and ω_2, are inserted into Eqs. 46 and 47, which provide the Kelvin-Voigt model parameters G' and η. The Bode diagram of the Kelvin-Voigt model with the new parameters is shown in Figure 6. The figure shows that G^*_{KV} intersects G^*_{E} at $\omega_1 = 0.2$ and at $\omega_2 = 1$. G^*_{KV} resembles G^*_{E} quite well also between these two frequencies.

In the phase shift plot of Figure 6, the two models intersect within the interval $[\,\omega_1\,,\,\omega_2\,]$. However, this is a coincidence that does not follow from the mathematical derivation. The phase shift diagrams of Figures 5 and 6 are almost identical. This is also a coincidence as the ratio $\frac{\eta}{G'}$ happens to be near identical in Example 3 and as in Example 2. End of Example 3.

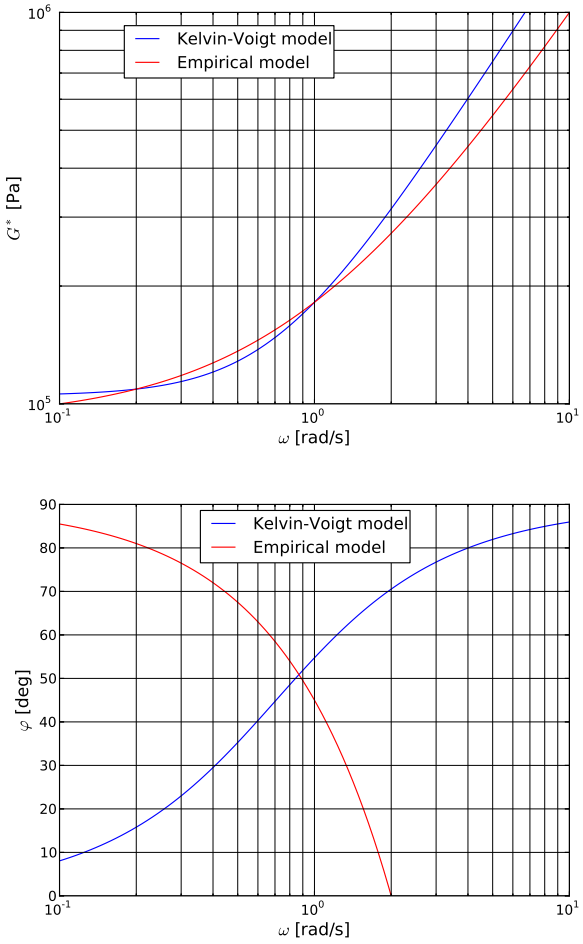

Figure 6. Bode diagram of the Kelvin-Voigt model obtained in Example 3.

It is seen from Figure 6 that the Kelvin-Voigt model underestimates G^* in the open interval $(\,\omega_1\,,\,\omega_2\,)$, and overestimates G^* for $\omega < \omega_1$ and for $\omega > \omega_2$. The following proves that this holds for any empirical model on the form of Eq. 17, and for any ω_1 and ω_2, provided that the parameter c_2 of the empirical model is positive.

It follows from Eq. 41 that $\frac{\mathrm{d}^2 G^*_{\mathrm{KV}}}{\mathrm{d}\omega^2}$ is positive for any finite ω. Hence, $\frac{\mathrm{d}G^*_{\mathrm{KV}}}{\mathrm{d}\omega}$ is strictly increasing. From Eq. 17 it follows that $\frac{\partial G^*_{\mathrm{E}}}{\partial \omega}$ is a positive constant w.r.t. ω.

The assumption of the present section is that $G^*_{\mathrm{KV}} = G^*_{\mathrm{E}}$ for the frequencies ω_1 and ω_2. That is

DOI 10.3384/ecp15119319

$$G^*_{\mathrm{KV}}(\omega_1) - G^*_{\mathrm{E}}(\omega_1) = 0, \tag{48}$$

$$G^*_{\mathrm{KV}}(\omega_2) - G^*_{\mathrm{E}}(\omega_2) = 0. \tag{49}$$

Rolle's theorem (see Section 4.2 of Thomas et al. (2010)) states that

$$\frac{\partial}{\partial\omega}\left[G^*_{\mathrm{KV}}(\omega_c) - G^*_{\mathrm{E}}(\omega_c)\right]\Big|_{\omega=\omega_c} = 0, \tag{50}$$

for some $\omega_c \in (\,\omega_1\,,\,\omega_2\,)$. Because $\frac{\mathrm{d}G^*_{\mathrm{KV}}}{\mathrm{d}\omega}$ is strictly increasing and $\frac{\partial G^*_{\mathrm{E}}}{\partial\omega}$ is constant, it follows that

$$\frac{\partial}{\partial\omega}\left[G^*_{\mathrm{KV}}(\omega) - G^*_{\mathrm{E}}(\omega)\right] < 0 \,\forall\, \omega < \omega_c, \tag{51}$$

$$\frac{\partial}{\partial\omega}\left[G^*_{\mathrm{KV}}(\omega) - G^*_{\mathrm{E}}(\omega)\right] > 0 \,\forall\, \omega > \omega_c. \tag{52}$$

Further,

$$G^*_{\mathrm{KV}}(\omega) = G^*_{\mathrm{KV}}(\omega_1) + \int_{\omega_1}^{\omega} \frac{\mathrm{d}G^*_{\mathrm{KV}}}{\mathrm{d}\omega}\,\mathrm{d}\omega, \tag{53}$$

$$G^*_{\mathrm{E}}(\omega) = G^*_{\mathrm{E}}(\omega_1) + \int_{\omega_1}^{\omega} \frac{\partial G^*_{\mathrm{E}}}{\partial\omega}\,\mathrm{d}\omega. \tag{54}$$

Subtracting Eq. 54 from Eq. 53, and using Eq. 48 gives

$$G^*_{\mathrm{KV}}(\omega) - G^*_{\mathrm{E}}(\omega) = \int_{\omega_1}^{\omega} \frac{\partial}{\partial\omega}\left[G^*_{\mathrm{KV}}(\omega) - G^*_{\mathrm{E}}(\omega)\right]\mathrm{d}\omega. \tag{55}$$

From Eq. 51 it follows that the integrand of Eq. 55 is negative if $\omega < \omega_c$. Hence, the integral is negative if $\omega_1 < \omega \leq \omega_c$, and it is positive if $\omega < \omega_1$. Therefore,

$$G^*_{\mathrm{KV}}(\omega) - G^*_{\mathrm{E}}(\omega) > 0 \;\forall \omega < \omega_1, \tag{56}$$

$$G^*_{\mathrm{KV}}(\omega) - G^*_{\mathrm{E}}(\omega) < 0 \;\forall \omega \in (\,\omega_1\,,\,\omega_c\,]. \tag{57}$$

A similar reasoning for $\omega > \omega_c$ gives

$$G^*_{\mathrm{KV}}(\omega) = G^*_{\mathrm{KV}}(\omega_2) + \int_{\omega_2}^{\omega} \frac{\mathrm{d}G^*_{\mathrm{KV}}}{\mathrm{d}\omega}\,\mathrm{d}\omega, \tag{58}$$

$$G^*_{\mathrm{E}}(\omega) = G^*_{\mathrm{E}}(\omega_2) + \int_{\omega_2}^{\omega} \frac{\partial G^*_{\mathrm{E}}}{\partial\omega}\,\mathrm{d}\omega. \tag{59}$$

Subtracting Eq. 59 from Eq. 58, and using Eq. 49 gives

$$G^*_{\mathrm{KV}}(\omega) - G^*_{\mathrm{E}}(\omega) = \int_{\omega_2}^{\omega} \frac{\partial}{\partial\omega}\left[G^*_{\mathrm{KV}}(\omega) - G^*_{\mathrm{E}}(\omega)\right]\mathrm{d}\omega. \tag{60}$$

By Eq. 52 the integrand of Eq. 60 is positive for $\omega > \omega_c$. Therefore, the integral is positive if $\omega > \omega_2$, and negative if $\omega_c \leq \omega < \omega_2$. Hence,

$$G^*_{\mathrm{KV}}(\omega) - G^*_{\mathrm{E}}(\omega) > 0 \;\forall \omega > \omega_2, \tag{61}$$

$$G^*_{\mathrm{KV}}(\omega) - G^*_{\mathrm{E}}(\omega) < 0 \;\forall \omega \in [\,\omega_c\,,\,\omega_2\,). \tag{62}$$

Combining Eqs. 56 and 57 with Eqs. 61 and 62 gives

$$G^*_{\mathrm{KV}}(\omega) < G^*_{\mathrm{E}}(\omega) \;\forall \omega \in (\,\omega_1\,,\,\omega_2\,), \tag{63}$$

$$G^*_{\mathrm{KV}}(\omega) > G^*_{\mathrm{E}}(\omega) \;\forall \omega \notin [\,\omega_1\,,\,\omega_2\,]. \tag{64}$$

This derivation proves that the Kelvin-Voigt model will always underestimate G^* between the frequencies ω_1 and ω_2. Further, the Kelvin-Voigt model will always overestimate G^* for frequencies smaller than ω_1 and larger than ω_2. In some applications it will be conservative to use large G^*. In these cases, the Kelvin-Voigt model will be non-conservative for frequencies between ω_1 and ω_2.

Subtracting Eq. 48 from Eq. 49, dividing by $\omega_2 - \omega_1$, and rewriting yields

$$\frac{G^*_{\mathrm{KV}}(\omega_2) - G^*_{\mathrm{KV}}(\omega_1)}{\omega_2 - \omega_1} = \frac{G^*_{\mathrm{E}}(\omega_2) - G^*_{\mathrm{E}}(\omega_1)}{\omega_2 - \omega_1}. \tag{65}$$

Taking the limit $\omega_2 \to \omega_1$

$$\lim_{\omega_2\to\omega_1} \frac{G^*_{\mathrm{KV}}(\omega_2) - G^*_{\mathrm{KV}}(\omega_1)}{\omega_2 - \omega_1} = \lim_{\omega_2\to\omega_1} \frac{G^*_{\mathrm{E}}(\omega_2) - G^*_{\mathrm{E}}(\omega_1)}{\omega_2 - \omega_1}, \tag{66}$$

$$\frac{\mathrm{d}G^*_{\mathrm{KV}}}{\mathrm{d}\omega}\Big|_{\omega=\omega_1} = \frac{\partial G^*_{\mathrm{E}}}{\partial\omega}\Big|_{\omega=\omega_1}. \tag{67}$$

Eq. 67 in combination with Eq. 48 state that the method of Section 5.2 is a special case of the method derived in the present section: Taking the limit $\omega_2 \to \omega_1$ of the method of the present section gives the method of Section 5.2.

6 Further Work

The work presented in this paper, together with the work presented in Olsen et al. (2014), Konradsen and Ouren (2014), and Komperød et al. (2015), are part of Nexans

Norway AS' effort to include the viscoelastic properties of bitumen in models of subsea cables and umbilicals.

The work of the present paper will be continued by modeling the mechanical properties of subsea cables and umbilicals with bitumen-coated armor wires using the UFLEX2D software. Because UFLEX2D requires bitumen's viscoelastic properties to be modeled by the Kelvin-Voigt model, the results of this paper are essential for modeling the effect of bitumen using UFLEX2D.

7 Conclusion

The contribution of the present paper is to evaluate the Kelvin-Voigt model's suitability to describe the viscoelastic properties of bitumen used as corrosion protection in subsea cables and umbilicals. This work is based on an empirical model developed by the author and his colleagues. This empirical model is published in Komperød et al. (2015).

The empirical model shows that bitumen's viscoelastic properties depend on the shear strain amplitude, shear strain rate, and the temperature. The Kelvin-Voigt model structure is not able to include dependence to strain amplitude nor to temperature. The lack of temperature dependence can be handled in the Kelvin-Voigt model by using different model parameters for different temperatures or by letting these model parameters be temperature-dependent, because it is reasonable (with a few exceptions) to assume that the bitumen temperature is homogeneous over one pitch length of the cable. The lack of strain amplitude dependence is a bigger issue, because bitumen's strain amplitude varies significantly within one pitch length of the cable. No solution to this issue has been found, except for choosing the Kelvin-Voigt parameters conservatively.

Under the assumption of constant strain amplitude, bitumen's frequency dependence in the Kelvin-Voigt model is analyzed and compared to the empirical model using Bode diagrams. Three different approaches are derived and discussed for how to decide the Kelvin-Voigt model parameters in order to resemble the frequency dependence of the empirical model. It is concluded that the Kelvin-Voigt model can resemble the shear stress amplitude to shear strain amplitude ratio and the phase shift between shear stress and shear strain at one single frequency. Alternatively, the Kelvin-Voigt model can resemble the shear stress amplitude to shear strain amplitude ratio over a limited frequency interval if the phase shift is disregarded. It is not possible to resemble the phase shift for more than a single frequency, because the derivative of the phase shift w.r.t. the frequency in the Kelvin-Voigt model inherently has opposite sign (plus or minus) compared to the empirical model.

References

J. J. Féret and C. L. Bournazel. Calculation of stresses and slip in structural layers of unbonded flexible pipes. *Journal of Offshore Mechanics and Arctic Engineering*, 109:263 – 269, 1987.

J. Hedlund. Modelling of viscoelastic dynamic bending stiffness for VIV analysis of submarine cables. In *Proceedings of the 9th International Conference on Insulated Power Cables (Jicable '15)*, 2015.

E. Kebadze. *Theoretical modelling of unbonded flexible pipe cross-sections*. PhD thesis, South Bank University, 2000.

M. Komperød, B. Konradsen, and R. Slora. Viscoelastic large strain model of bitumen used for corrosion protection in subsea cables and umbilicals. In *Proceedings of the ASME 2015 34th International Conference on Ocean, Offshore and Arctic Engineering OMAE 2015*, 2015.

B. Konradsen and S. V. Ouren. Modeling the effects of temperature and frequency on bitumen-coated helical cable elements. In *Proceedings of the 55th Conference on Simulation and Modelling (SIMS 2014) - Aalborg, Denmark*, 2014.

J. Mullins, D. Morin, A. Tyrberg, C. Sonesson, and J. Ekh. Bitumen shear mechanics in a dynamic subsea electrical cable. In *Proceedings of the ASME 2015 34th International Conference on Ocean, Offshore and Arctic Engineering OMAE 2015*, 2015.

A. Nysveen, H. Kulbotten, J. K. Lervik, A. H. Børnes, M. Høyer-Hansen, and J. J. Bremnes. Direct electrical heating of subsea pipelines - Technology development and operating experience. *IEEE Transactions on Industry Applications*, 43:118 – 129, 2007.

E. Olsen, K. A. Hansen-Zahl, and S. Karlsen. Viscoelastic behaviour of bitumen in dynamic control umbilicals. In *Proceedings of the ASME 33rd International Conference on Ocean, Offshore and Arctic Engineering OMAE 2014*, 2014.

G. B. Thomas, M. D. Weir, and J. Hass. *Thomas' calculus - global edition - 12th edition*. Pearson Education, Inc., 2010.

A About UFLEX2D

The UFLEX program system originates from a joint MARINTEK and Nexans Norway AS effort kicked off in 1999, resulting in a 2D software module (UFLEX2D) for structural analysis of complex umbilical cross-sections. The first version of the tool was launched in 2001. From 2005 and onwards further development of the 2D module as well as the development of a 3D module (UFLEX3D) has taken place within a Joint Industry Project (JIP). The JIP is still running, and is financed by a group of 10 sponsors covering the following oil and gas industry segments; operators, suppliers, technical service providers.

DOI 10.3384/ecp15119319